24. D. Kasper *et al.*, *EMBO J.* **24**, 1079 (2005).
25. P. F. Lange, L. Wartosch, T. J. Jentsch, J. C. Fuhrmann, *Nature* **440**, 220 (2006).
26. S. Weinert *et al.*, *Science* **328**, 1401 (2010); published online 29 April 2010 (10.1126/science.1188072).
27. M. Saito, P. I. Hanson, P. Schlesinger, *J. Biol. Chem.* **282**, 27327 (2007).
28. We thank R. Pareja-Alcaraz and S. Rode for technical assistance and P. Verroust, S. Bachmann, W. Blaner, and C. Wagner for antibodies against cubilin, megalin, retinol binding protein, and AE1, respectively. This work was supported by the Deutsche Forschungsgemeinschaft (grants Zd58/1, Je164/6, and Je164/9).

Supporting Online Material
www.sciencemag.org/cgi/content/full/science.1188070/DC1
Materials and Methods
Figs. S1 to S8
Table S1
References

8 February 2010; accepted 21 April 2010
Published online 29 April 2010;
10.1126/science.1188070
Include this information when citing this paper.

Lysosomal Pathology and Osteopetrosis upon Loss of H^+-Driven Lysosomal Cl^- Accumulation

Stefanie Weinert,[1,2] Sabrina Jabs,[1,2,6] Chayarop Supanchart,[3] Michaela Schweizer,[4] Niclas Gimber,[1,2] Martin Richter,[1,6] Jörg Rademann,[1,6]* Tobias Stauber,[1,2] Uwe Kornak,[3,5] Thomas J. Jentsch[1,2]†

During lysosomal acidification, proton-pump currents are thought to be shunted by a chloride ion (Cl^-) channel, tentatively identified as ClC-7. Surprisingly, recent data suggest that ClC-7 instead mediates Cl^-/proton (H^+) exchange. We generated mice carrying a point mutation converting ClC-7 into an uncoupled (unc) Cl^- conductor. Despite maintaining lysosomal conductance and normal lysosomal pH, these *Clcn7*$^{unc/unc}$ mice showed lysosomal storage disease like mice lacking ClC-7. However, their osteopetrosis was milder, and they lacked a coat color phenotype. Thus, only some roles of ClC-7 Cl^-/H^+ exchange can be taken over by a Cl^- conductance. This conductance was even deleterious in *Clcn7*$^{+/unc}$ mice. *Clcn7*$^{-/-}$ and *Clcn7*$^{unc/unc}$ mice accumulated less Cl^- in lysosomes than did wild-type mice. Thus, lowered lysosomal chloride may underlie their common phenotypes.

ClC-7 is the only member of the CLC gene family of anion transporters substantially expressed on lysosomes (*1*–*3*), where it resides together with its β-subunit Ostm1 (*3*). Inactivation of either subunit leads to lysosomal storage disease and osteopetrosis in mice and humans (*1*–*4*). Cellular defects include slowed degradation of endocytosed proteins (*5*) and impaired acidification of the osteoclast resorption lacuna (*1*). Cl^- currents mediated by ClC-7 have been deemed necessary for shunting lysosomal proton-pump currents (*1*). However, lysosomal pH was normal in cells lacking either ClC-7 or Ostm1 (*2*, *3*). ClC-7 now seems likely to be a Cl^-/H^+ exchanger rather than a Cl^- channel (*6*, *7*). Because H^+-pump currents may be neutralized by both Cl^- channels and electrogenic Cl^-/H^+ exchangers (*6*), it is unclear whether lysosomal Cl^-/H^+ exchange confers functional advantages over the simple Cl^- conductance in the textbook model for vesicular acidification.

We created knock-in mice in which the ClC-7 "gating" glutamate (E) was mutated to alanine (A) (fig. S1) (*8*). On the basis of results from other CLC Cl^-/H^+ exchangers (*9*–*12*), this $Glu^{245} \rightarrow Ala^{245}$ (E245A) mutation should lead to Cl^- transport that is uncoupled (unc) from protons, hence our designation of this allele as *Clcn7*^{unc}. Homozygous *Clcn7*$^{unc/unc}$ mice showed severe growth retardation (Fig. 1A and fig. S2) and died within 5 weeks. ClC-7^{unc} and wild-type (WT) ClC-7 were expressed at similar levels (Fig. 1B) and similarly localized to lysosomes (Fig. 1D). Neither the abundance, nor the lysosomal localization of Ostm1 was changed in *Clcn7*$^{unc/unc}$ mice, contrasting with its strongly reduced protein level (*3*) and mislocalization in *Clcn7*$^{-/-}$ cells (Fig. 1, C and D). In neurons, however, ClC-7^{unc} staining was more diffuse (fig. S3B), reflecting changed lysosomal compartments like in *Clcn7*$^{-/-}$ neurons (*2*). The abundance of other CLC exchangers was unchanged in *Clcn7*$^{unc/unc}$ mice (fig. S4).

In an *agouti* genetic background, the coat color of *Clcn7*$^{-/-}$ and *Ostm1*$^{-/-}$ (*grey-lethal*) mice is grey (*3*, *4*), whereas it was brownish in WT and *Clcn7*$^{unc/unc}$ mice (Fig. 1A). *Clcn7*$^{unc/unc}$ mice were osteopetrotic (Fig. 2A and fig. S5), although less severely than *Clcn7*$^{-/-}$ (*1*) or *Ostm1*$^{-/-}$ (*4*) mice. ClC-7 and Ostm1 were detected at the ruffled border of *Clcn7*$^{unc/unc}$ osteoclasts (fig. S3A). This

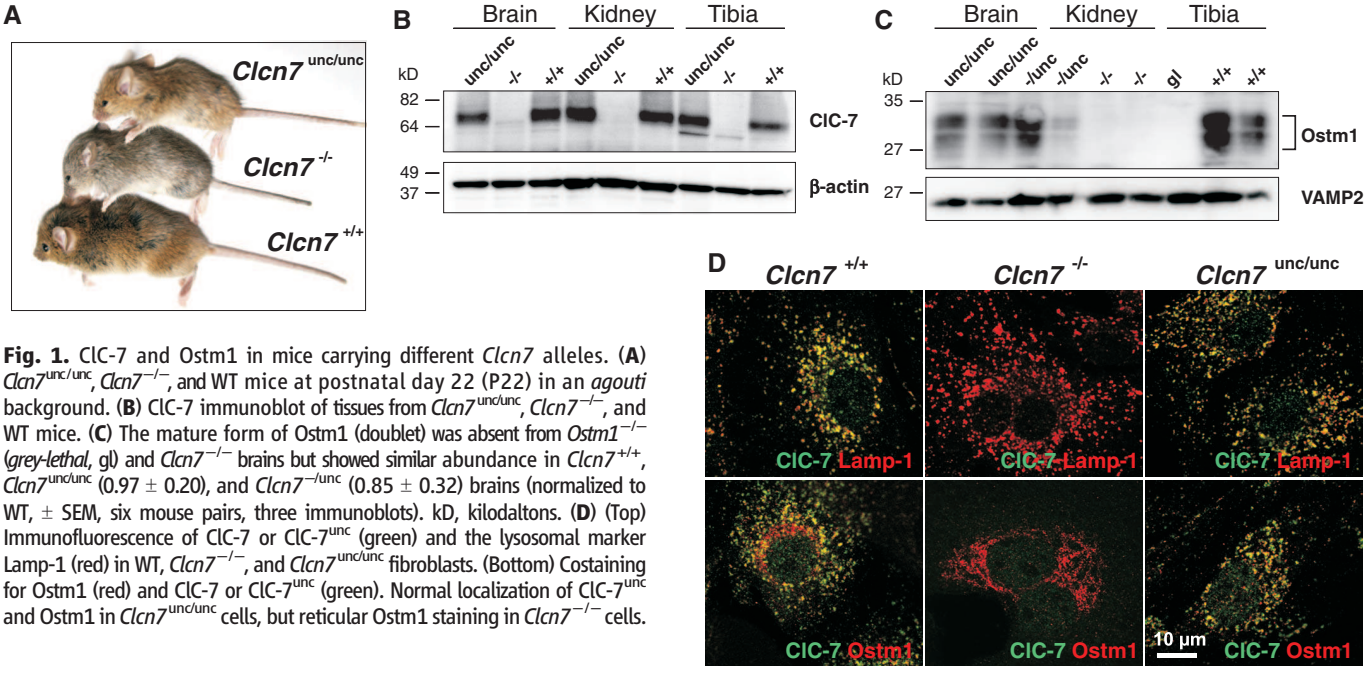

Fig. 1. ClC-7 and Ostm1 in mice carrying different *Clcn7* alleles. (**A**) *Clcn7*$^{unc/unc}$, *Clcn7*$^{-/-}$, and WT mice at postnatal day 22 (P22) in an *agouti* background. (**B**) ClC-7 immunoblot of tissues from *Clcn7*$^{unc/unc}$, *Clcn7*$^{-/-}$, and WT mice. (**C**) The mature form of Ostm1 (doublet) was absent from *Ostm1*$^{-/-}$ (*grey-lethal*, gl) and *Clcn7*$^{-/-}$ brains but showed similar abundance in *Clcn7*$^{+/+}$, *Clcn7*$^{unc/unc}$ (0.97 ± 0.20), and *Clcn7*$^{-/unc}$ (0.85 ± 0.32) brains (normalized to WT, ± SEM, six mouse pairs, three immunoblots). kD, kilodaltons. (**D**) (Top) Immunofluorescence of ClC-7 or ClC-7^{unc} (green) and the lysosomal marker Lamp-1 (red) in WT, *Clcn7*$^{-/-}$, and *Clcn7*$^{unc/unc}$ fibroblasts. (Bottom) Costaining for Ostm1 (red) and ClC-7 or ClC-7^{unc} (green). Normal localization of ClC-7^{unc} and Ostm1 in *Clcn7*$^{unc/unc}$ cells, but reticular Ostm1 staining in *Clcn7*$^{-/-}$ cells.

acid-secreting membrane was underdeveloped in *Clcn7*$^{unc/unc}$ and almost lacking in *Clcn7*$^{-/-}$ osteoclasts (Fig. 2B). WT, *Clcn7*$^{-/-}$, and *Clcn7*$^{unc/unc}$ osteoclasts similarly attached to dentine and established actin rings that surround resorption lacunae (fig. S6A). In contrast to almost nonresorbing *Clcn7*$^{-/-}$ osteoclasts (*1*), *Clcn7*$^{unc/unc}$ osteoclasts excavated pits, albeit their number and depths were strongly reduced (Fig. 2C and fig. S6B).

Like mice lacking ClC-7 (*2*) or Ostm1 (*3*), *Clcn7*$^{unc/unc}$ mice displayed rapidly progressing retinal degeneration (fig. S7) and developed neurodegeneration with features of lysosomal storage disease (Fig. 2D and fig. S8). Although *Clcn7*$^{+/unc}$ mice lacked an obvious phenotype during the first 5 months, they showed slowly progressing hippocampal neurodegeneration (Fig. 2D and fig. S8C). No such degeneration was seen in *Clcn7*$^{+/-}$ mice.

To examine whether the E245A mutation had converted ClC-7 from a Cl^-/H^+ exchanger into an uncoupled anion conductor, we exposed fluorescein-dextran–loaded lysosomes to different external Cl^- concentrations ($[Cl^-]_o$) in the presence of K^+ and valinomycin to shunt currents. Cl^-/H^+ exchange predicts a more alkaline luminal pH (pH_l) with higher $[Cl^-]_o$. Changes in $[Cl^-]_o$ induced larger pH_l differences in WT than in *Clcn7*$^{unc/unc}$ or knockout (KO) lysosomes (Fig. 3A), suggesting that ClC-7 mediates Cl^-/H^+ exchange, which is uncoupled by the E245A mutation. The Cl^--dependent pH_l changes remaining with KO and *Clcn7*$^{unc/unc}$ lysosomes might be owed to a partial shift of late endosomal ClC-3 into lysosomes as in *Clcn7*$^{-/-}$ mice (*13*).

We then added the proton ionophore carbonyl cyanide 3-chlorophenylhydrazone (CCCP) to cultured fibroblasts whose lysosomes were preloaded with a pH indicator. CCCP dissipates lysosomal pH only in the presence of countercurrents. Lysosomes from all three genotypes rapidly alkalinized upon CCCP addition (Fig. 3B). *Clcn7*$^{unc/unc}$ lysosomes reached a more alkaline pH_l than *Clcn7*$^{-/-}$ lysosomes. Thus, ClC-7^{unc} mediates a conductance that is most likely carried by Cl^- as in equivalent mutants of other CLC exchangers (*9*–*12*). Although biophysics predicts identical equilibrium pH_l with an H^+ leak parallel to either a Cl^- conductance or a $2Cl^-/H^+$ exchanger (fig. S9), steady-state pH_l was less alkaline in *Clcn7*$^{unc/unc}$ than in WT lysosomes (Fig. 3B). Because equilibrium H^+-gradients are determined by the Cl^- diffusion potential, this pH_l difference suggests higher lysosomal chloride concentration ($[Cl^-]_l$) in WT than in *Clcn7*$^{unc/unc}$ lysosomes. The CCCP-induced alkalinization of *Clcn7*$^{-/-}$ lysosomes (Fig. 3B) indicates the presence of a sizable lysosomal conductance beyond ClC-7. The final pH of CCCP-treated KO lysosomes, which is more acidic than that of *Clcn7*$^{unc/unc}$ lysosomes, might be explained by a lumen-negative potential created by a cation conductance (fig. S9). Mixed K^+/Na^+ conductances were reported for lysosomes (*14*).

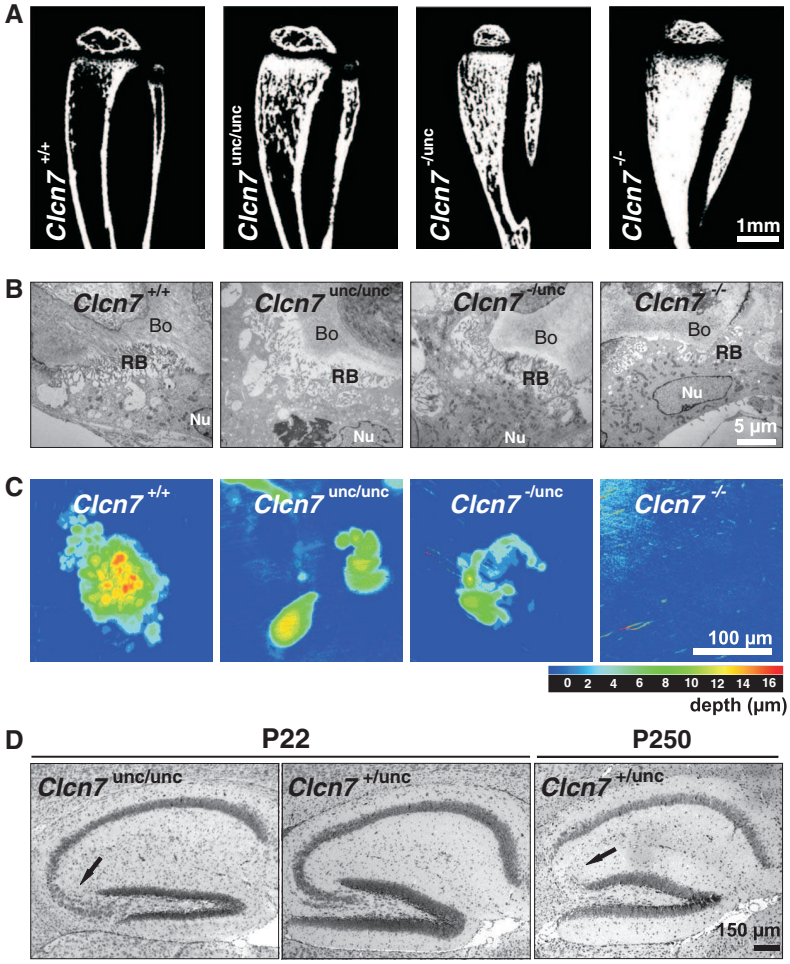

Fig. 2. Bone and brain phenotypes. (**A**) Micro–computed tomography images of tibiae showed increasing severity of osteopetrosis from *Clcn7*$^{unc/unc}$ over *Clcn7*$^{-/unc}$ to *Clcn7*$^{-/-}$ mice. (**B**) Electron micrographs reveal underdeveloped ruffled borders in osteoclasts of *Clcn7*$^{unc/unc}$ and *Clcn7*$^{-/unc}$ mice. *Clcn7*$^{-/-}$ osteoclasts lacked those membranes almost completely (Bo, bone; Nu, nucleus; RB, ruffled border). (**C**) *Clcn7*$^{unc/unc}$ and *Clcn7*$^{-/unc}$ osteoclasts excavated shallower resorption pits into dentine than WT, with only superficial resorption found with *Clcn7*$^{-/-}$ osteoclasts. Mean pit depths (± SEM): 12.2 ± 1.0 µm (*Clcn7*$^{+/+}$, n = 25 pits), 6.0 ± 0.8 µm (*Clcn7*$^{unc/unc}$, n = 34), 3.7 ± 0.5 µm (*Clcn7*$^{-/unc}$, n = 21), and 0.1 ± 0.1 µm (*Clcn7*$^{-/-}$, n = 5). (**D**) Nissl staining of P22 brain sections showing neuronal cell loss (arrows) in the hippocampal CA3 region in *Clcn7*$^{unc/unc}$ but not in *Clcn7*$^{+/unc}$ mice, which showed degeneration at P250.

As predicted by sizable lysosomal conductances in all three genotypes, fluorescein-dextran–loaded lysosomes of WT, *Clcn7*$^{unc/unc}$, and *Clcn7*$^{-/-}$ mice showed adenosine triphosphate (ATP)–driven acidification in vitro (Fig. 3C). Agreeing with the presence of a cation conductance, *Clcn7*$^{-/-}$ lysosomes acidified also without $[Cl^-]_o$ (Fig. 3C). The marked difference to renal endosomes, whose acidification depends on chloride and ClC-5 (*15*–*17*), may be explained with a larger cation conductance in lysosomes (*14*).

We ratiometrically measured pH in lysosomes of fibroblasts that were loaded with the dextran-coupled pH indicator Oregon Green 488 by endocytosis. There was no measurable difference between *Clcn7*$^{unc/unc}$, *Clcn7*$^{+/unc}$, *Clcn7*$^{+/+}$, or *Clcn7*$^{-/-}$ cells (Fig. 3D). The normal steady-state pH_l and robust ATP-dependent acidification eliminates lysosomal pH as an important factor in lysosomal pathology of *Clcn7*$^{unc/unc}$ and *Clcn7*$^{-/-}$ mice.

To better understand the role of Cl^-/H^+ exchange in vesicular acidification, we modeled a minimal vesicle containing just an H^+ pump, an H^+ leak, and either a $2Cl^-/H^+$ exchanger or a Cl^- channel. Although H^+ exits through the antiporter during acidification, simulations predicted more efficient acidification with the exchanger (fig. S10A). Whereas the lumen became positive in the classical model involving a Cl^- channel (*18*), it got negative with the exchanger (fig. S10B). This surprising prediction might solve the mystery shrouding the voltage-dependence of endosomal ClC-4 and -5 [thought to be almost inactive at lumen-positive voltages

[1]Leibniz-Institut für Molekulare Pharmakologie (FMP), 13125 Berlin, Germany. [2]Max-Delbrück-Centrum für Molekulare Medizin (MDC), 13125 Berlin, Germany. [3]Institut für Medizinische Genetik, Charité Universitätsmedizin, 13353 Berlin, Germany. [4]Zentrum für Molekulare Neurobiologie (ZMNH), Universität Hamburg, 20251 Hamburg, Germany. [5]Max-Planck-Institut für Molekulare Genetik, 14195 Berlin, Germany. [6]Freie Universität, 14195 Berlin, Germany.

*Present address: Institut für Pharmazie, Universität Leipzig, 04103 Leipzig, Germany.
†To whom correspondence should be addressed. E-mail: jentsch@fmp-berlin.de

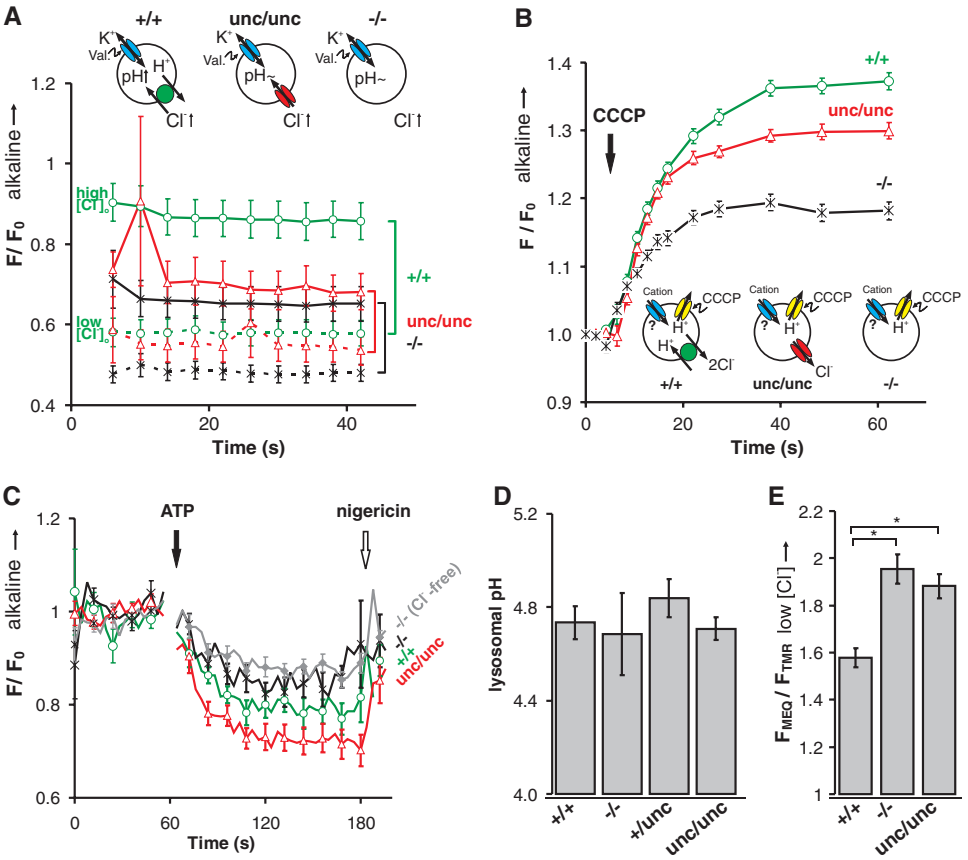

Fig. 3. Lysosomal transport characterization. (**A**) The unc mutation abolished ClC-7 Cl^-/H^+ exchange, as revealed by Cl^--gradient–driven pH changes in fluorescein-dextran–loaded lysosomes exposed to low (10 mM, dashed lines) or high (107 mM, solid lines) $[Cl^-]_o$ in vitro. Averages from 42 (+/+), 20 (unc/unc), and 32 (–/–) experiments are shown. F, ratio of fluorescence at λ = 535 nm obtained with excitation at 488 and 440 nm; F_0, F at time t = 0; Val., valinomycin. (**B**) CCCP-induced alkalinization of lysosomes in fibroblasts monitored by Oregon Green–dextran fluorescence. Means from more than five independent cell lines per genotype, with >100 lysosomes from eight cells each. (**C**) Similar ATP-dependent acidification in vitro of *Clcn7*$^{+/+}$, *Clcn7*$^{unc/unc}$, and *Clcn7*$^{-/-}$ lysosomes (the latter with and without Cl^-). The K^+/H^+-exchanger nigericin was added as a control. Means from 14 (+/+), 14 (unc/unc), 10 (–/–), and 23 (–/–, Cl^--free) experiments are shown. Error bars (indicating SEM) are shown for every third data point. (**D**) Steady-state pH_l in WT, *Clcn7*$^{-/-}$, *Clcn7*$^{+/unc}$, and *Clcn7*$^{unc/unc}$ fibroblasts. Averages from three independent cell lines per genotype, with ~100 lysosomes from three cells each, are shown. (**E**) Lower $[Cl^-]_l$ in *Clcn7*$^{-/-}$ and *Clcn7*$^{unc/unc}$ than in *Clcn7*$^{+/+}$ lysosomes revealed by chloride-sensitive fluorescence ratio of MEQ/tetramethylrhodamine-dextran endocytosed by fibroblasts and chased 2 hours into lysosomes in medium containing 7 mM Cl^-. Means from ≥10 experiments are shown (three cell lines per genotype, 10 cells with 10 lysosomes each per experiment). *P < 0.001, Student's t test. Error bars denote SEM throughout.

(*10*, *11*, *19*)], but it conflicts with the general view that endosomes and lysosomes are positive inside (*20*–*22*). Thus, considering the effects of Cl^-/H^+ exchange on vesicular voltage might be worthwhile.

On the basis of our calculations, we predicted that vesicles accumulate more Cl^- with a Cl^-/H^+ exchanger than with a Cl^- conductor (fig. S10C). We synthesized a dextran-coupled, ratioable Cl^--sensitive dye (fig. S11) and loaded it into lysosomes of fibroblasts. The strongly quenched fluorescence of its Cl^--sensitive 6-methoxy-N-ethylquinolinium bromide (MEQ) moiety in WT, KO, and *Clcn7*$^{unc/unc}$ lysosomes indicated high $[Cl^-]_l$ in all genotypes, but the low sensitivity of the dye above ~60 mM $[Cl^-]$ (fig. S11) precluded reliable comparisons of $[Cl^-]_l$. When we shifted $[Cl^-]_l$ into a measurable range by preincubating cells in low chloride, significantly lower MEQ quenching (lower $[Cl^-]_l$) was detected in *Clcn7*$^{-/-}$ and *Clcn7*$^{unc/unc}$ than in WT lysosomes (Fig. 3E). Analogous to this ClC-7–dependent Cl^- accumulation into mammalian lysosomes, plant vacuoles may use AtClC-a to accumulate nitrate (*23*).

Our work has several implications for lysosomal biology. The central nervous system and bone pathology of *Clcn7*$^{-/-}$ mice is not due to a loss of Ostm1 that is unstable without ClC-7 (*3*). However, the stronger bone phenotype and changed coat color of mice lacking ClC-7/Ostm1 (table S1) might indicate that protein-protein interactions, which are almost certainly unchanged in the E245A mutant, play a role in those phenotypes. Alternatively, the conductance mediated by ClC-7^{unc} may partially substitute for Cl^-/H^+ exchange in these tissues. This might occur in the acidification of the osteoclast resorption lacuna (*1*), either directly by shunting H^+-currents or by facilitating the exocytic build-up of the ruffled border. Furthermore, the *Clcn7*^{unc} allele has dominant phenotypical effects. The ClC-7^{unc} conductor may recycle Cl^- for the ClC-7 Cl^-/H^+ exchanger, thereby creating the equivalent of an H^+-leak in *Clcn7*$^{+/unc}$ mice. Finally, for supporting proper lysosome and osteoclast function, it is not sufficient that ClC-7 mediates electrical currents but must exchange chloride for protons. The biological importance of lysosomal Cl^-/H^+ exchange may be related to H^+-gradient–driven anion accumulation.

References and Notes

1. U. Kornak *et al.*, *Cell* **104**, 205 (2001).
2. D. Kasper *et al.*, *EMBO J.* **24**, 1079 (2005).
3. P. F. Lange, L. Wartosch, T. J. Jentsch, J. C. Fuhrmann, *Nature* **440**, 220 (2006).
4. N. Chalhoub *et al.*, *Nat. Med.* **9**, 399 (2003).
5. L. Wartosch, J. C. Fuhrmann, M. Schweizer, T. Stauber, T. J. Jentsch, *FASEB J.* **23**, 4056 (2009).
6. T. J. Jentsch, *J. Physiol.* **578**, 633 (2007).
7. A. R. Graves, P. K. Curran, C. L. Smith, J. A. Mindell, *Nature* **453**, 788 (2008).
8. Materials and methods are available as supporting material on *Science* Online.
9. A. Accardi, C. Miller, *Nature* **427**, 803 (2004).
10. A. Picollo, M. Pusch, *Nature* **436**, 420 (2005).
11. O. Scheel, A. A. Zdebik, S. Lourdel, T. J. Jentsch, *Nature* **436**, 424 (2005).
12. E. Y. Bergsdorf, A. A. Zdebik, T. J. Jentsch, *J. Biol. Chem.* **284**, 11184 (2009).
13. M. Poët *et al.*, *Proc. Natl. Acad. Sci. U.S.A.* **103**, 13854 (2006).
14. R. W. Van Dyke, *Am. J. Physiol.* **265**, C901 (1993).
15. W. Günther, N. Piwon, T. J. Jentsch, *Pflügers Arch.* **445**, 456 (2003).
16. M. Hara-Chikuma, Y. Wang, S. E. Guggino, W. B. Guggino, A. S. Verkman, *Biochem. Biophys. Res. Commun.* **329**, 941 (2005).
17. G. Novarino, S. Weinert, G. Rickheit, T. J. Jentsch, *Science* **328**, 1398 (2010); publshed online 29 April 2010 (10.1126/science.1188070).
18. M. Grabe, G. Oster, *J. Gen. Physiol.* **117**, 329 (2001).
19. K. Steinmeyer, B. Schwappach, M. Bens, A. Vandewalle, T. J. Jentsch, *J. Biol. Chem.* **270**, 31172 (1995).
20. B. E. Steinberg, N. Touret, M. Vargas-Caballero, S. Grinstein, *Proc. Natl. Acad. Sci. U.S.A.* **104**, 9523 (2007).
21. R. Fuchs, P. Mâle, I. Mellman, *J. Biol. Chem.* **264**, 2212 (1989).
22. S. Ohkuma, Y. Moriyama, T. Takano, *J. Biochem.* **94**, 1935 (1983).
23. A. De Angeli *et al.*, *Nature* **442**, 939 (2006).

24. We thank I. Freyert, A. von Bock, and P. Göritz for technical assistance; M. Falcke for help with modeling; and S. Grinstein for suggesting protonophore pretreatment of lysosomes. Support was provided by the Deutsche Forschungsgemeinschaft [grants Je164/7 and SFB740 (C5)] to T.J.J., SFB765(Ra895/6) to J.R., and the OSTEOPETR E-Rare grant (Bundesministerium für Bildung und Forschung) to UK

Supporting Online Material

www.sciencemag.org/cgi/content/full/science.1188072/DC1
Materials and Methods
Figs. S1 to S11
Table S1
References

8 February 2010; accepted 21 April 2010
Published online 29 April 2010;
10.1126/science.1188072
Include this information when citing this paper.